CASL-U-2014-0209-000

Power uprates
and plant life extension

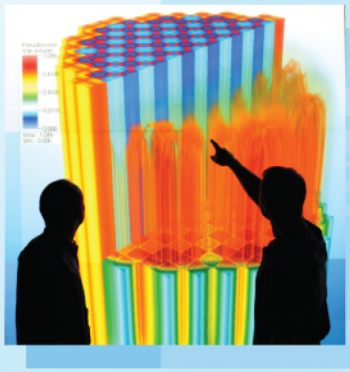

Engineering design
and analysis

Science-enabling
high performance
computing

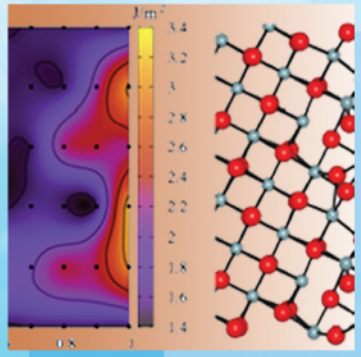

Fundamental science

Plant operational data

Consortium for Advanced Simulation of LWRs

L3:THM.CFD.P9.05

Full-Field Measurements of Turbulent Bubby Flow using Innovative Experimental Techniques

Yassin A. Hassan
Texas A&M University

September 30, 2014

U.S. DEPARTMENT OF ENERGY | Nuclear Energy

MILESTONE

FULL-FIELD MEASUREMENTS OF TURBULENT BUBBLY FLOW USING INNOVATIVE EXPERIMENTAL TECHNIQUES

Yassin A. Hassan

Texas A&M University – Nuclear Engineering Department
337 Zachry Engineering Building,College Station, TX, 77843-3133

y-hassan@tamu.edu

ABSTRACT

Multi-phase flows are one of the challenges on which the CFD simulation community has been working extensively with a relatively low success. The phenomena associated behind the momentum and heat transfer mechanisms associated to multi-phase flows are highly complex requiring resolving simultaneously for multiple scales on time and space. Part of the reasons behind the low predictive capability of CFD when studying multi-phase flows, is the scarcity of CFD-grade experimental data for validation. The complexity of the phenomena and its sensitivity to small sources of perturbations makes its measurements a difficult task. Non-intrusive and innovative measuring techniques are required to accurately measure multi-phase flow parameters while at the same time satisfying the high resolution required to validate CFD simulations. In this context, this work presents the implementation of innovative measuring techniques that can provide whole-field and multi-scale measurements of two-phase flow turbulence parameters. To this end, simultaneous implementation of visualization techniques are used to study isothermal two-phase turbulent flows through a vertical rectangular channel. These techniques are listed next and are used as follow: 1) Particle Tracking Velocimetry (PTV) is used to analyze the influence that the diluted phase parameters have on the liquid phase turbulence statistics, and 2) High-speed shadowgraphy with LED illumination is used to obtain the gas phase dynamics. The present experiments are intended to improve the understanding of two-phase turbulent flows and to provide reliable and accurate experimental information for verification and validation of two-phase flow computational models. In this report, isothermal bubbly turbulent flow in a square channel was studied. The experiments were performed with two different gases diluted in liquid refrigerant (3M-7000). Helium and nitrogen were used as the dispersed phase. The gas was injected into the channel through a porous media at three different superficial gas velocities. For helium, the gas superficial velocities were: 0.81 mm/s, 3.85 mm/s, 7.33 mm/s. And for nitrogen, the gas superficial velocity was 5.50 mm/s, 9.17 mm/s, 16.5 mm/s. Measurements of the liquid parameters

such as the velocity, RMS of the liquid velocity, and Reynolds stresses were provided by PTV. The availability of simultaneous shadowgraphy and PTV experiments allowed the study of the intricate interaction between the liquid and gas phases. The present experiments were designed to provide information for the development and validation of two phase flow turbulence models.

1. INTRODUCTION

The understanding of two-phase flow parameters and their impact on the liquid turbulence plays a key role on the behavior prediction, safety analysis and design of the high energy systems found in industry. In particular, the nuclear industry relies on the accurate prediction of local two-phase flow parameters. For example, the nucleation sites location and the amount of void within coolant/moderator sub-channels affect not only the reactor's reactivity, but also promote the crud formation which has been shown to contribute to the generation of heat transfer non-uniformities along the fuel rods and ultimately fuel rod structural failures. Although multiple experimental efforts has been directed towards the understanding of two-phase turbulent flow, the complexity of the phenomenon and its high dependence on the experimental conditions has produced large discrepancies among experimental results, even at similar conditions. Therefore there is a need of innovative experimental techniques that can fulfill the demanding statistical requirements to describe the stochastic nature of two-phase turbulent flows. This work explores the scope and limitations of innovative measuring techniques to study isothermal two-phase flows, in specific bubbly flow regimes. Emphasis is given to achieve measurements with the required temporal and spatial resolutions for both: average and fluctuating quantities. Multiple experimental efforts have been performed to obtain a better understanding of the parameters involved in two-phase flow by using different methods and techniques. Most of the important turbulence parameters have been measured using point intrusive methods. Normally, such instruments can achieve the required temporal resolution for the time scales found in many engineering systems. Based on probe point measurements from past experiments, models were created to compute two-phase flows (Roy et al., 2002; Yeoh et al., 2002, Končar et al., 2004, Ramstorfer et al., 2008). Since the intrusive techniques will not provide the spatial information, non-intrusive measurement methods were applied in two phase bubbly flow experiments. The recent development of high speed camera electronics, visualization techniques have evolved into powerful tools capable of delivering whole-field quantitative information with temporal resolutions comparable to that of point measurement techniques (Khan et al., 2011). Examples of such non-intrusive techniques include Particle Image Velocimetry (PIV), Particle Tracking Velocimetry (PTV), Laser Doppler Velocimetry (LDV), and Magnetic Resonance Velocimetry (MRV). Laser Induced Fluorescence (LIF) is another flow visualization technique which has been applied along with PIV to

measure two-phase flows (Sathe et al., 2010; Dahikar et al., 2010). Since the point measurement instruments are spatially limited, they are unable to provide whole-field (2-D) data which is essential for the complete description of the interaction between the phases. Shadowgraphy is a visualization technique that does not employ particle seedings or a laser as its illumination source. Usually, halogen lamps or LEDs (Light Emitting Diodes) are the light sources for illumination. This method does not require costly or high-powered lasers and is a simple method to obtain bubble dynamics information. It is a non-intrusive method and provides 2-D measurements of bubbles velocity, size, and void fraction distribution. Although the shadowgraphy technique has many advantages, it is limited only to relatively low void fraction cases, and requires efficient algorithms to reduce the influence of out of focus bubbles. Lindken and Merzkirch (2002) performed an experiment in which they applied similar visualization techniques as the ones used in the present study. They used PIV and shadowgraphy. They injected bubbles at a Reynolds number of 1,400 into a square tank filled with stagnant liquid and measured the bubble and liquid velocity with a camera. Even though they were able to measure the velocity of the two phases simultaneously, their results lacked information such as the distributions of void fraction and bubble size. Zaruba et al. (2005) measured the velocity and size of bubbles in a rectangular bubble column 10 cm in width and 2 cm in depth. The bubbles were inserted through an aquarium porous stone with a range of superficial gas velocities of 1-6 mm/s. The only method utilized was similar to shadowgraphy. The velocity was calculated by tracking the center of mass of the bubble. To measure the size of the bubble, a method was proposed in which only spherical and elliptical bubbles were considered. Due to its limitation, they concluded that the method would have to be improved. Their results did not include any information pertaining to the liquid velocity. Sathe and Thaker (2010) presented two phase bubbly flow experiments. Their work reports measurements of the shape, size, velocity and acceleration of bubbles using shadowgraphy and liquid velocity measurement obtained using PIV/LIF with fluorescent tracer particles. Measurements were performed in a narrow rectangular column at moderate gas hold-up (~5%) with wide variation of bubble sizes (0.1–15 mm). Broder and Sommerfeld (2008) adopted a combined system of PIV and PTV to measure bubble size, bubble velocity and liquid velocity in a double loop reactor. It was possible to determine bubble size distributions and mean, as well as fluctuating velocities for both phases. However, no laser was used in this study. The PIV was done on shadow image of particles. The narrow depth of focus of lens was relied upon to get planer velocity. There is noted that the out of focus bubbles were removed based on the intensity gradient at the interface of shadow image. Hammad (2010) adopted an experimental procedure based on a combination of PIV, shadowgraphy and PTV to investigate bubbly flows. The procedure is applied to the turbulent two-phase flow arising from the normal impingement of a round free-surface water jet on a horizontal air-water interface. A fully developed turbulent jet, exiting a long pipe, ensured properly characterized inflow conditions. Time-resolved particle tracking velocimetry (TR-PTV) and shadowgraphy techniques were used to measure the velocity and size distributions of

the dispersed phase. An elaborate post processing procedure was used for background equalization, noise removal, threshold detection, gradient analysis and validation. The image processing and evaluation scheme included the detection of each bubble contour, centroid, shape, size and particle tracking-based velocity determination. A threshold level parameter was used to define the contours of the bubbles in the images. Edge height/slope validation criteria were used to accept well focused bubbles.

Near Wall Measurements and Modeling

From experimental information researches had explore the relationship between the gas phase parameters and the near-wall liquid velocity. Although the scarcity of detailed experimental information is evident, multiple efforts for the modeling and prediction of two-phase flows have been performed. Here we present a summary of previously proposed models and simulation studies, emphasizing those focusing on the development of a near-wall liquid velocity model. Marie et al. (1997a) performed experiments of a turbulent boundary layer developing on a vertical flat plate in the presence of millimeter bubbles. For the bubble frequency and void fraction measurements they used a single-probe optical sensor with a measuring volume of the order of $(50\ \mu\mathrm{m})^3$, and a high speed camera to measure average bubble velocity, size and shape. For the liquid measurements, they used a miniature conical hot-film anemometer with a sensitive ring size of about 0.1 mm. Also, using a wall flush-mounted hot-film sensor they measured the wall shear stress at a station located at 1m from the leading edge. From their detailed measurements, they found that the behaviour of the liquid velocity in the near-wall region consisted on the three regions also found in the single-phase boundary layer theory; the viscous sublayer, logarithmic zone and the wake region were still preserved for their bubbly flows, at least for the void fractions they considered (α < 7%). They showed that the measured two-phase friction velocity (U'_*) cannot be considered as a velocity scale for the description of the level of shear stress in the near-wall region, instead, a new two-phase flow velocity scale was proposed (U'^x_*) which accounted for the modification of the friction at the surface and the differential gravity forces acting between the wall and the free-stream bubble layers with $U'^{x2}_* = U'^2_* - g(\epsilon_* - \epsilon_E)\bar{D}_B$ on which ϵ_* and ϵ_E represent the near-wall and the free stream average bubble void fraction values, and $\bar{D}_B$ represents the average bubble diameter. Hence, Marie et al. proposed a modified law of the wall $U^{+x} = U_L/U'^x_* = 1/\kappa^x \ln(y^{+x}) + B^x$ with coefficients κ^x and B^x which depend also on the void fraction profile and the average bubble diameter. Relevant of the proposed model is the fact that the slope of the logarithmic law remains unchanged, while its origin is shifted upward depending on the void fraction.Gabillet et al. (2002) performed bubbly flow experiments through a horizontal channel to simulate the effects of wall bubble nucleation and departure through a porous plate in the lower wall. To measure the void fraction, bubble velocity and diameter they used a fibre-optic probe. The liquid-phase parameters were measured with a hot film anemometry down to a minimum distance from the

wall of about $y = 0.75$ mm ($y^+ = 45$) due to the probe size restrictions. They showed a self-similar behaviour of the void fraction profiles proportional to the initial void fraction at the injection position (α_0) and the axial distance (x). They also found that the velocity profiles follow a logarithmic law with a behaviour similar to surface roughness studies, suggesting that bubbles acted as roughness elements on the liquid flow. From these observations and from the mixture momentum equation they concluded that a new velocity scale ($U_*^{'x}$) and a new additive constant (B^x) were needed. Their proposed velocity scale being a function of the single-phase friction velocity (measured from pressure measurements), the bubble layer thickness, and the initial void fraction at the injection position $U_*^{'x} = f(U_*, \delta^{'}, \alpha_0)$. The new additive constant was defined as a function of the new friction velocity and the indirect measure of the bubble diameter through the bubble induced roughness height $B^x = f(U_*', k_B)$. With their proposed logarithmic function they obtained similar results as Marie et al., in the sense that the slope of the logarithmic law remained unchanged, however the profile origin shifted downwards instead of upwards. In other modeling efforts,Troshko & Hassan (2001b) developed a two-phase logarithmic law of the wall for isothermal bubbly turbulent boundary layers. They defined a velocity scale similar to the one used by Marie et al. ($U_*^{\prime x} = \beta U_*'$) with a different proportionality factor (β) function of the slip and friction velocity, void fraction, and the Von Karman constant $\beta = f(U_r, U_*', \alpha_{max}, \kappa)$. with a slip velocity given by $U_r = (4g\sigma\Delta\rho/\rho_l)^{1/4}(1 - \alpha_m ax)^{3/4}$. An important part of their model was a correction for high void fraction cases on which the linear superposition assumption of the total turbulent viscosity was under question. This correction was included into the β proportionality factor with the term $\kappa_l = 4.9453\exp(-40.661 \cdot U_*')$ which was empirically obtained from the experimental results of Marie et al. (1997a). Using perturbation theory, Mikielewicz (2003) developed a near wall function for isothermal bubbly flows based on the asymptotic correction methodology. He proposed two approaches, one on which the void fraction distribution was assumed constant and the other with a model to predict the wall peaking effect for the condition evaluated. The assumption of a constant void fraction led to a logarithmic function dependent on gas phase parameters such as the void fraction, bubble diameter, and the bubble drag coefficient, while the dependence on the liquid parameters was introduced by the relative velocity and the friction velocity $U_+^x = f(\alpha, D_B, C_D, U_r, U_*')$. Worth noting is the use of different values for the additive constant ($B^x = 7.7$), and for the location of the transition between the viscous and the logarithmic layers from $y_+^0 = 11$ to a value of $y_+^0 = 8$, these values justified from the assumption that at locations bellow y_+^0 no bubbles should exist. Mikielewicz tested his approaches against the experimental data of Marie et al. (1997a) and found that while there was not a significant difference between the two proposed approaches, both improved the prediction of the two-phase liquid velocity compared to single-phase models. Based on the idea originally proposed by Gabillet et al. (2002) of considering nucleating bubbles as a surface roughness, Ramstorfer (2007) proposed a model for

subcooled flow boiling. Firstly, they performed boiling flow experiments through a horizontal channel of about 36×36 mm^2. They used high speed visualization to measure bubble size and dynamics, and a 2D laser-Doppler anemometer for the liquid velocity measurements. Two important differences to (Gabillet et al. 2002) approach consisted on the fact that the additive constant ($B^x = B = 5.45$) was left unchanged; instead a new additive term was included (Δu^+) which depended on a bubble equivalent roughness defined as $k_B = \eta \bar{D}_B (q_{nb}/q_w)^\xi$ being η and ξ coefficients determined experimentally and q_{nb}/q_w representing the ratio of nucleate boiling component to the total heat flux through the heater wall, Ramstorfer (2007) obtained, for each condition, the value of the required velocity scale (U_*') and the value of the bubble equivalent roughness (k_B) from fitting the surface roughness law of the wall to the experimental data. Their results show a similar behavior to those on isothermal bubbly flows in a horizontal arrangement with a constant slope and a downward shift proportional to the bubble diameter and void fraction. Aligning their modeling to the roughness theory, they defined a velocity scale for boiling conditions function of the bulk velocity (U_b) and a friction coefficient (f) as $U_*'^x = \sqrt{f/8}\, U_b$ where f is a modified version of the Colebrook and White's friction universal formula (Colebrook 1939), which is dependent on the bubble equivalent roughness. They found that the proposed model was limited to predict conditions of high bulk velocities on which the bubble buoyancy effects on the liquid velocity can be considered negligibly small. To predict the conditions on which the model is valid, they proposed a non dimensional map using the Froude (Fr) and the (Ja) Jakob number. They found an empirical expression for the boundary that separates the buoyancy independent from the buoyancy dependent regimes, which reads $Fr = [1 - 0.47 \log(Ja)]^{-1}$. A summary of some of the proposed two-phase flow models to describe near-wall velocity is depicted in Table . It is important to note that regardless of the nature of the system, isothermal bubbly flow or boiling flow, the preferred model is of logarithmic nature. The analogy to the single phase case of different regions still holds, with slight variations on the location dividing the viscous sublayer and the logarithmic region, either $y_+^0 = 11$ or $y_+^0 = 8$, these values being somehow arbitrary. Nevertheless the models seem to provide reasonable improvements when comparing to single phase models. Two approaches have been identified, the first approach is the extension of the single phase mixing length theory to predict two phase flows, and the second approach is an analogy to the roughness theory in turbulent flows through channels. Common to these models is the fact that they are based on experimental measurements on which buoyancy effects are much smaller than inertial forces; therefore, considering slow moving bubbles as equivalent roughness in the wall is justified. Also most of the included physics that describe the bubble behavior are based on a balance of forces that a single bubble is subject to, (drag forces, lift forces, buoyancy forces, etc.), however the experimental works used on the development of these models are limited and these assumptions cannot be explicitly tested. Remarkably, multiple attempts have been made to modify the isothermal two-phase flow models to be

used on boiling flow modeling (Koncar & Krepper 2008; Koncar & Tiselj 2010; Ramstorfer 2007). From these works Ramstorfer et al. (2008) has been the only researchers who performed boiling experiments to support their proposed model. However, they used boiling bubbles as tracers to acquire their liquid velocity measurements, this under the assumption of a zero slip velocity between the phases. This indeed may produce undesirable velocity bias when the bubbles buoyancy play a significant role, consequently, his model is restricted to conditions of high Reynolds numbers and relatively small void fractions.

Table 1 Summary of proposed near-wall functions for two-phase flow simulations

Parameter	Marie (1997)	Troshko (2001)	Mikielewics (2003)	Ramstorfer (2008)
general form	$U_+^x = \frac{1}{\kappa^x}\ln\left(y_+^x\right) + B^x$	$U_+^x = \frac{1}{\kappa^x}\ln\left(y_+^x\right) + B^x$	$U_+^x = -\frac{1}{\kappa^x}\ln\left(\kappa^x/y_+^x + M\alpha\kappa^4\right) + B^x$	$U_+^x = \frac{1}{\kappa^x}\ln\left(y_+^x\right) + B^x - \Delta U_+^x$
velocity scale	$U_*'^x = \beta U_*'$	$U_*'^x = \beta U_*'$	$U_*'^x = U_*'$	$U_*'^x = \sqrt{f/8}\, U_b$
correction factor	$\beta = \left[1 - \left(g\frac{D_B}{U_*'^2}\right)(\epsilon_P - \epsilon_E)\right]^{1/2}$	$\beta = \left[\left(1 + \frac{\kappa_l \alpha_{\max} U_r}{\kappa U_*'}\right)(1 - \alpha_{\max})\right]^{-1}$	$\beta = (1-\alpha)^{1/2}$	$f = \left[-2\log\left(\frac{2.51}{\mathrm{Re}\sqrt{f}} + 0.27 C_{\mathrm{kr}c}\frac{k_r^+}{D_h}\right)\right]^{-2}$
additive constant	$B^x = B + y_+^0\left(\frac{1}{\beta} - 1\right) - \frac{1}{\kappa}\ln(\beta)$	$B^x = y_+^0(1-\beta) + \beta B$	$B^x = 7.7$	$B^x = B$
Von Karman constant	$\kappa^x = \beta^{-1}\kappa$	$\kappa^x = \kappa\beta^{-1}$	$\kappa^x = \beta\kappa$	$\kappa^x = \kappa$
end of viscous layer	$y_+^0 \approx 11$	$y_+^0 \approx 11$	$y_+^0 \approx 8$	$y_+^0 \approx 11$
$U_+^x = U_L/U_*'^x$	$y_+^x = yU_*'^x/\nu$	$\kappa_l = 4.9453\mathrm{e}^{-40.661U_*'}$	$M = \frac{3}{4}\frac{C_D U_r}{D_B}\frac{\nu}{\kappa^2 U_*'^4}$	$\Delta u_+^x = \frac{1}{\kappa}\ln(1 + C_{\mathrm{kr}}k_r^+),\ k_r^+ \geq 90$
$\kappa \approx 0.419$	$B \approx 5.45$	$U_r = [4g\sigma\Delta\rho/\rho_l]^{1/4}(1-\alpha_{\max})^{3/4}$	$C_D = \frac{24(1+0.15\mathrm{Re}^{0.687})}{\mathrm{Re}_b}\left(1 + \frac{0.02D_B}{y}\right)$	$k_r^+ = \eta\bar{D}_B\left(\frac{q_{nb}}{q_w}\right)^{\xi}$
$C_{\mathrm{kr}c} \approx 0.65$	$C_{\mathrm{kr}} \approx 0.65$		$U_r = \left[\frac{2\sigma}{\rho_l D_B} + \frac{\Delta\rho g D_B}{2\rho_l}\right]^{1/2}$	

Common to all previous proposed models are the efforts to develop a near-wall function based on a logarithmic model assumption. This is indeed a common sense choice, considering how well the law of the wall predicts single phase turbulent flows. However, such assumption has led to new and different constants or empirical correlations among researchers. Some of the inconsistencies among these models are due in part to the lack of detailed experimental information. Two-phase turbulent flow phenomenon complexity does not easily allow measuring the relationship between the phases in a simultaneous and instantaneous manner. Most of the experimental data on flow boiling are non-simultaneous average measurements of either the liquid and/or the gas phases (Lee et al. 2002; Roy et al. 2002; Yeoh et al. 2002), making it difficult to find proper relationships between them. This lack of detailed information is part of the motivation of this work. Due to experimental and technical difficulties, most of these studies are often oriented to measure parameters of only one phase, i.e. either liquid or vapour parameters, with experimental approaches that are also limited to offer either long-term averages, such as average void fraction distribution, average velocity profiles, etc. or instantaneous or fast occurring events, such as bubbles departure frequency, bubble growth rate, instantaneous liquid vorticity fields, etc. Furthermore, there had been limited attempts to capture simultaneously the full-field wall heat transfer mechanisms and the interaction with the liquid and vapor dynamics. The present has the objective of extending the measurements capabilities to overcome some of the limitations as to include simultaneous PTV-Shadowgraphy to fully account for local and global changes present in two-phase turbulent flows. This work is an attempt to provide high-quality

data of isothermal two-phase flow for validation and improvement of two phase flow computational models.

2. EXPERIMENTAL SETUP

The experimental facility was designed for the visualization of two-phase flow regimes with refrigerant HFE-301 at low system pressure. The facility consists of a hydraulic loop and a visualization system. Experimental setup details are given in the following sections.

Hydraulic Loop

The hydraulic loop consists of an external loop and a test section, both designed to withstand temperatures in excess of 200 ^{o}C, and pressures up to 100 psi. The external loop provides thermal and hydraulic steady state conditions. The system excess energy is removed with a small plate heat exchanger connected to a chilling system. This allows us to have control of the inlet temperature to the test section. The mass flow rate to the test section was measured with a Coriolis flow meter and controlled by adjusting the test section valves. The test section is a rectangular channel made of transparent polycarbonate, with 30.5 cm length and a cross-sectional area of 10 x 10 mm^2 Figure 1 shows the schematics of the hydraulic system and the dimensions of the test section.

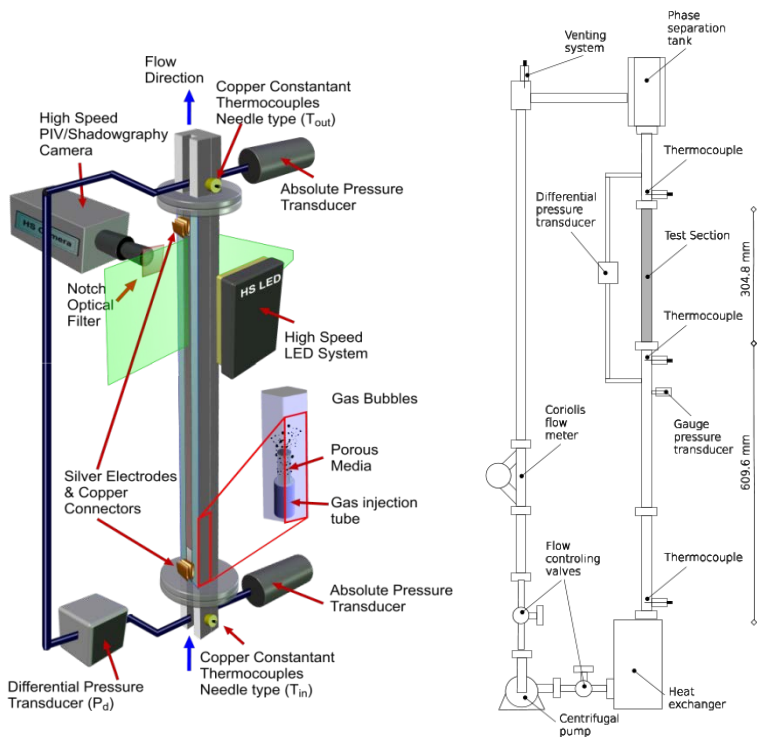

Figure 1 Test section (left), hydraulic loop (right).

Visualization System

The visualization system consisted of a high-speed high-resolution camera, a high-speed high-power laser, a fast response LED illumination system, mirrors, translational stages, lenses, optical filters and particle flow tracers. The flow tracers are fluorescent particles with density range of 1.39 to 1.41 g/cm, with an average particle diameter of 5 μm. The high-speed camera has a maximum frame rate of 6000 fps at a resolution of 1024x1024 pixels, with a maximum bit depth of 12 bits. The illumination was provided by a Pegasus dual lamp laser which can operate at a maximum power of 27 mJ/pulse. A maximum pulse rate of 20,000 pulse/s can be achieved. Two optical mirrors and two concave-convex lenses are used to convert the small circular beam from the laser, into a thin sheet of light. The laser light sheet is positioned on the measurement region, parallel to the camera focal area. The LED system is externally synchronized to be used as the shadowgraphy illumination. The camera, mirrors and lenses are mounted on translational stages to have the capability of changing the measuring region along the test section. The camera, the laser and the LED illumination system are synchronized in such a way as to be able to obtain quasi-simultaneous PTV and Shadowgraphy images. This experimental configuration was designed to have multi-scale measurements. The high speed PIV-Shadowgraphy camera is arranged to provide "semi-simultaneous" measurements of PTV and shadowgraphy images. This is achieved by synchronizing the camera shutter with alternating pulses of laser and led illumination. From the temporal multi-scale point of view, the camera can be configured to run in continuous or in straddling modes. Continuous mode provides a fixed time interval between each consecutive frame. In order to properly capture the fast moving features within the flow, this time interval (Δt_{PIV}) need to be small and consequently the camera need to be run at high speeds. Due to the camera memory limitations the continuous configuration provides short measuring times of the order of fractions of a second. Straddling mode combines a small time interval (small Δt_{PIV}) between image pairs plus a waiting period which will be called straddling time ($\Delta t_{Straddling}$). This waiting period is required to acquire a higher number of independent samples while increasing the measuring interval. Similarly, the two high speed shadowgraphy images can also be configured to work in either continuous or straddling modes. To achieve spatial multi-scale measurements, the PTV-Shadowgraphy camera is used with a telecentric lens which allow the selection of different visualization modes

3. EXPERIMENTS

PTV-Shadowgraphy experiments

The measurement area was located at about 23 cm from the test section inlet. Simultaneous PTV and shadowgraphy measurements were performed at this position with a single high-speed camera. The

high-speed camera frame rate was set to 8,400 frames/s, with an exposure time of 150 μs. The relatively large exposure rate was selected as to allow enough light to reach the camera sensor and achieve satisfactory shadowgraphs of the bubbles. Each acquired image consisted of 1024×1024 pixels. Two kinds of gases, nitrogen and helium were used as the diluted phase. The gas was injected through an injection system from the bottom of the channel. The injection system consists of a coarse porous media with an average porous size of 40 μm and a diameter of 0.7mm. The flow rate was controlled and monitored by the coriolis flow meter. The selected flow rates for helium, were, 2.2 sccm, 12.5 sccm, and 25 sccm. While the selected flow rates for nitrogen, were 15 sccm, 25 sccm, and 42.5 sccm. The liquid flow rate was fixed in all cases with a value of 0.061 l/s which is equivalent to a Reynolds of 6500. For all cases a constant inlet temperature of 15 ^{o}C was maintained. Inlet and outlet fluid temperatures were also measured by means of thermocuples to ensure isothermal conditions. Schematically, **Figure 3** shows the considered gas flow conditions.

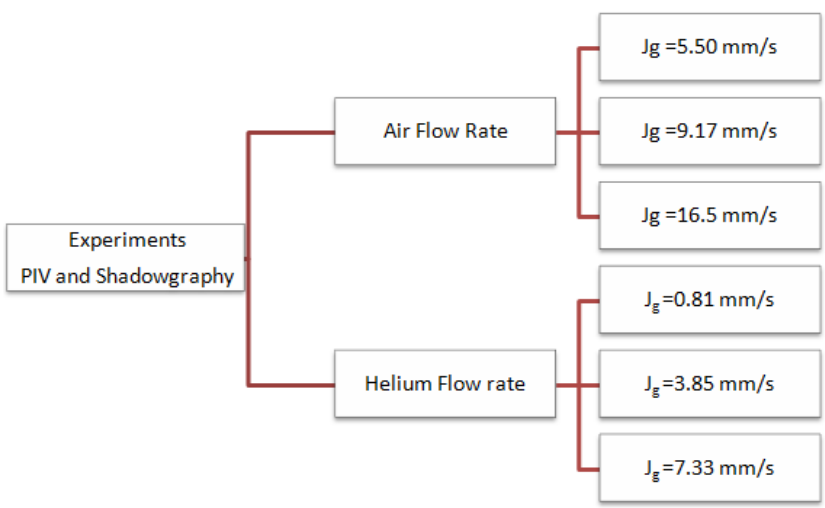

Figure 2 Schematics of experimental matrix

Figure 3 shows an example of the simultaneous PIV-Shadowgraphy measurements. Figure 3a shows the image obtained with the laser light ilumination. This is the PIV image which provide information for the liquid velocity measuements. It is important to mention that the camera lens is equiped with a notch filter with a band pass within the range 532 +/- 15 nm. The notch filter blocks most of the laser ligth, and therefore helps to reduce the undesired reflections from the bubbles. This in turns allows a

more accurate liquid velocity measurement, since the spurius vectors produced by the bubbles reflections are notabely reduced. Figure 3b shows the images acquired with the LED ilumination. These are the shadowgraphy images which will provide the gas phase dynamics. By combining the information from the PIV and shadowgraphy images, a more faithful liquid velocity measurement can be obtained. The bubbles images from the shadowgraphy frames are used to reduce even more the bubbles reflections that are still present in the PIV frame. This will provides a cleaner version of the PIV image on which the bubbles reflections are efficiently removed. The PTV analysis of the "clean" PIV frame is shown in Figure 3c. No velocity vectors were obtained at positions fully occupied by bubbles, confirming that only the liquid velocity is being tracked.

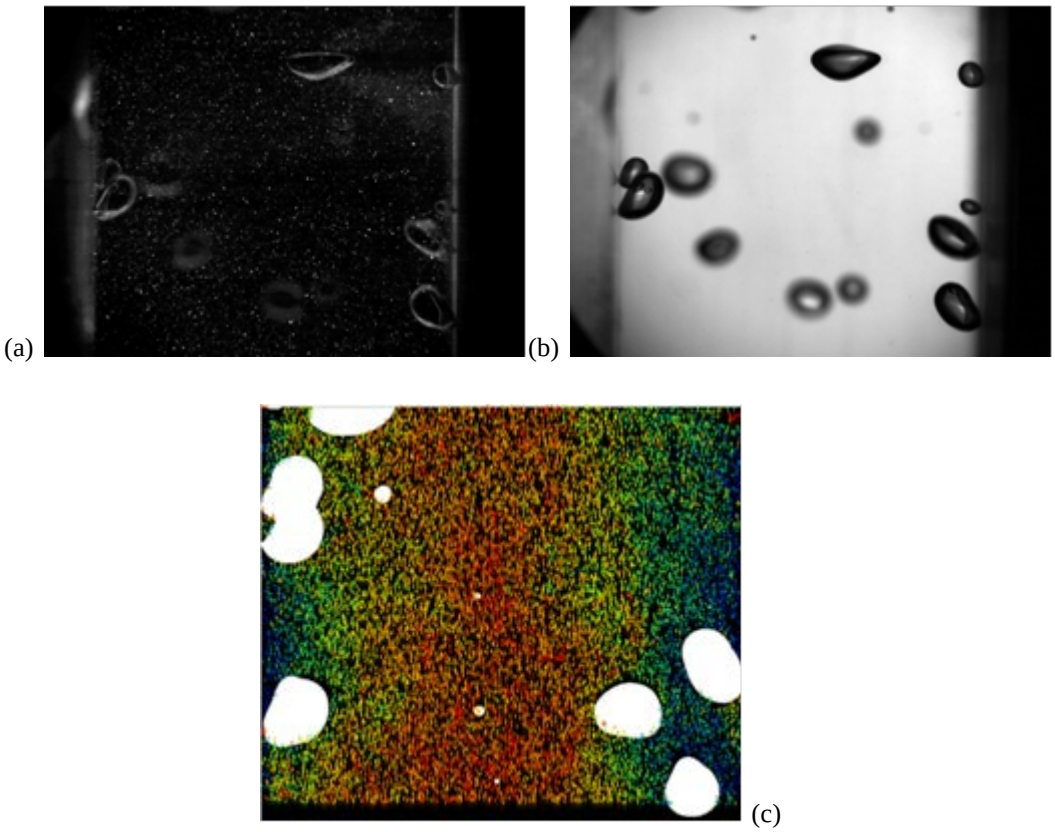

Figure 3 Experimental results showing a) PIV image, b) Shadowgraphy image c) Velocity field obtained with PTV.

To achieve accurate liquid velocity results such as the ones shown in Figure 4(c) several image pre-processing and post-processing algorithms were developed. In this study, the PTV algorithm used to obtain the liquid velocity measurements is a home-developed routine that has been applied successfully in several previous two-phase flow investigations (Hassan et al., 2005; Dominguez-Ontiveros et al., 2006; OrtizVillafuerte and Hassan, 2006). The original algorithm was developed by

Canaan and Hassan (1991), and has been improved over the years. A simplified version of the PTV algorithm performs: (1) image pre-processing, (2) particle detection, (3) particle centroid location estimation and (4) particle matching (tracking) between consecutive frames. The components of the PTV algorithm that are new or relevant for the present study are described: Image pre-processing is useful to modify the raw-data coming directly from the camera memory. The commonly applied image pre-processing is the subtraction of an average image set. This procedure greatly reduces the camera noise and common reflections from the channel walls. Another typical procedure is the application of spatial-filters such as the Gaussian smoothing. This image pre-processing is selected because it is compatible with the particle detection algorithm which looks for Gaussian image features for accurate particle centroid location. The final goal of the image pre-processing is to facilitate the object centroid and tracking procedures. Proper implementation of image pre-processing can reduce significantly peak locking effects and improve the subpixel interpolation. The image pre-processing is depicted in Figure 4(a). (2) The next step is the particle centroid location algorithm. The particle detection procedure is particularly important in multi-phase flow experiments where accurate identification and discrimination between phases is required. In this study a particle mask correlation method (Takehara, 1998) is implemented. This technique is an image template matching routine, where the selected template is generated from a Gaussian representation of an ideal particle. (3) Once a particle is identified, its centroid is estimated to sub-pixel accuracy. In this study three different centroid estimation techniques are available: three point Gaussian interpolation (3PGI) (Willert and Gharib, 1991), two-dimensional Gaussian regression (2DGR) (Noback and Honkanen, 2005), and center of mass technique (CMT). 3PGI and 2DGR performance and accuracy are similar as both are well suited for small (radius <10 pixels) Gaussian shaped objects. The CMT is better suited for larger objects (radius >10 pixels) without shape restriction. In a two-phase flow PTV experiment, CMT will be ideal for the location of bubbles centroid, while 3PGI and 2DGR are well suited to estimate the liquid tracer particles centroids. Although 3PGI technique is the most commonly used among researchers due to its simplicity, in this work, 2DGR is preferred since it relies on more information (9 pixels are used in the regression rather than 6) to estimate the centroids. (4) The particle tracking algorithm is based on direct spatial correlation. This algorithm computes a correlation coefficient between two sub-images of single-exposed PTV pictures. The correlation coefficient will determine which particle in one frame is the best match of a particle on the next frame. Since particles location is estimated to sub-pixel accuracy, and the interval between pictures is known, accurate particle velocity estimation can be achieved.

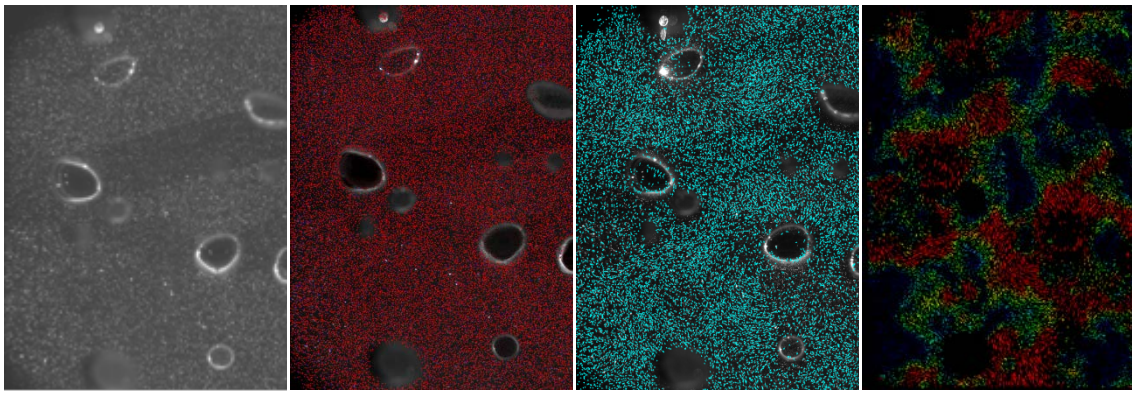

(a) Image pre processing | (b) *Particle centroid location* | (c) *Particle Tracking* | (d) *Liquid velocity statistics*

Figure 4 Liquid velocity measurements procedure.

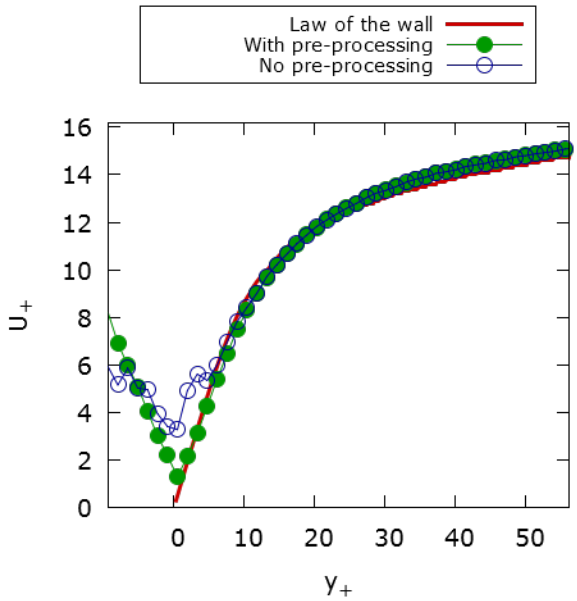

Figure 5 Comparison of near-wall liquid velocity measurements with and without image processing

Axial liquid velocity modification

One of the main objectives of the PTV measurements is to obtain detailed information of the liquid velocity close to the wall under isothermal bubbly flow conditions. Figure 11 shows the average axial velocity profile for different gas superficial velocities. It is important to remark that the velocity

profiles did not showed to be symmetric; this was the result of a small bias on the location of the porous media. Although, to reduce the effect of the injection system on the liquid statistics we could have located the porous media farther from the measurement area, however we were restricted because the flow regime changed with the distance. Since we required studying bubbly flow regime, this distance has to be small. Therefore the effects of the liquid turbulence due to the injection system were still present. Nevertheless, the influence of the void fraction on the liquid velocity is clear. There is a shifting upwards of the whole profile with void fraction. This results are similar to those obtained by previous researchers (Marie et al. 1997b), and showed to be different to the behavior previously found in subcooled flow boiling (Estrada-Perez & Hassan 2010; Hasan et al. 1992; Ramstorfer et al. 2008; Roy et al. 1993). This is explained because the bubbles domains in subcooled flow boiling mostly stay in the near-wall region. The gas phase in bubbly flow experiments are evenly distributed through the flow domain, therefore the gas phase can have an effect in the whole velocity profile. To have a better understanding of the liquid behavior, it is always convenient to present these results in dimensionless form. The characteristic length and velocity used for the non-dimensionalization are $y^+ = (yu_\tau)/\nu$ for the characteristic length and u_τ for the characteristic velocity, u_τ is the friction velocity defined as $u_\tau = \sqrt{(\tau_w/\rho)}$. The wall shear stress (τ_w) is obtained experimentally using the approximation for regions close to the wall as $\tau_w = \mu\, du/dy|_{y=0}$. Using the single phase frictional velocity Figure 11 shows the non-dimensional form of the axial velocity profile for different superficial gas velocities. From this plot it is clear a significant difference from the single case (shown in red). These differences are attributed to the gravity driven flow induced in the vicinity of the bubbles.

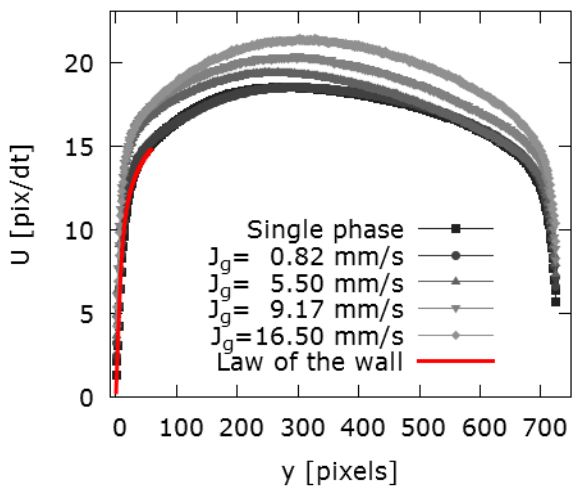

Figure 6 Axial liquid velocity profile at different axial positions from the nucleation site.

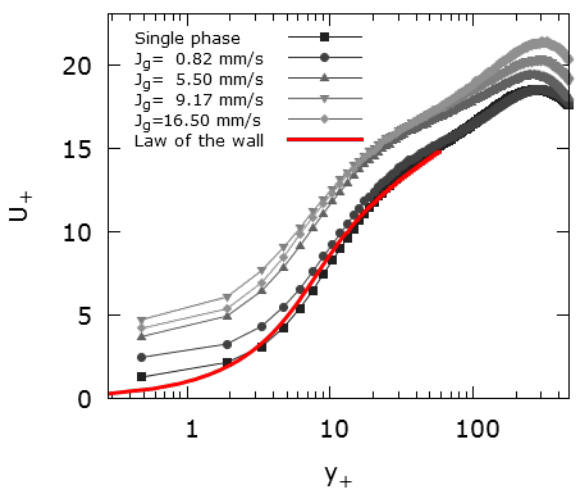

Figure 7 Semi-log plot of the axial liquid velocity profile at different axial positions from the nucleation site using the single-phase friction velocity as a velocity scale.

To further gain insight on the effect of the bubbles parameters on the liquid turbulence, the two phase friction velocity (u_*^x) was estimated by three different approaches, namely: The wall-slope method, the Durst polynomial fitting, and from direct differential pressure measurements. These techniques are well documented and validated for single phase conditions (Durst et al. 1996) , extending these approaches to be implemented in a two-phase condition remains a question. However, these techniques has been previously tested in two-phase flow conditions with some success (Dominguez-Ontiveros et al. 2006) . The wall-slope method and the Durst polynomial approach rely on the accurate estimation of the near wall velocity measurements by the PTV algorithm. The Durst method showed to be less sensitive to the selected points to perform the curve fitting, as long as the velocity information was bellow $y_+ < 12$. It is important to note that although significant discrepancies between the Durst and the wall-slope method were found, these measurements were within the differential pressure measurement uncertainty range, giving us some degree of confidence on these results. Also it is important to recall that the wall-slope and Durst methods provide a detailed description of the wall shear stress local change along the measurement area. In this scenario, the differential pressure measurements provide only the average wall shear stress, which is useful for the local wall shear stress measurements validation.

By using the measured two-phase flow friction velocity the new non-dimensional plot of the liquid velocity profiles are shown in Figure 12. The resulting trend is similar to what Marie et al. (1997a) found when using two-phase friction velocity measurements from a wall shear stress sensor. There appears to be a profile downward shifting with an increase of the void fraction. This suggested that the direct use of the measured two-phase friction velocity measurements is not a proper approach to fully characterize the subcooled boiling data. Furthermore, previous studies ((Koncar & Tiselj 2010; Marie et al. 1997a; Troshko & Hassan 2001a) had focused on the logarithmic layer modeling, i.e. for $y_+ > 30$ and neglecting the viscous sublayer due probably to the lack of experimental data in the near-wall region. The simplifying assumption was that a similar dynamics structure prevails for both the single and the two-phase flow conditions. However, when looking to more detailed experimental information it is clear that the viscous sublayer is also affected by the bubbles presence, and this changes cannot longer be ignored.

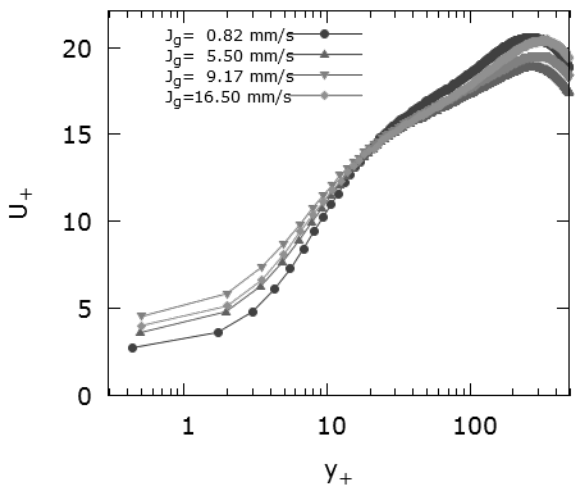

Figure 8 Semi-log plot of the axial liquid velocity profile at different axial positions from the nucleation site using the two-phase friction velocity as a velocity scale.

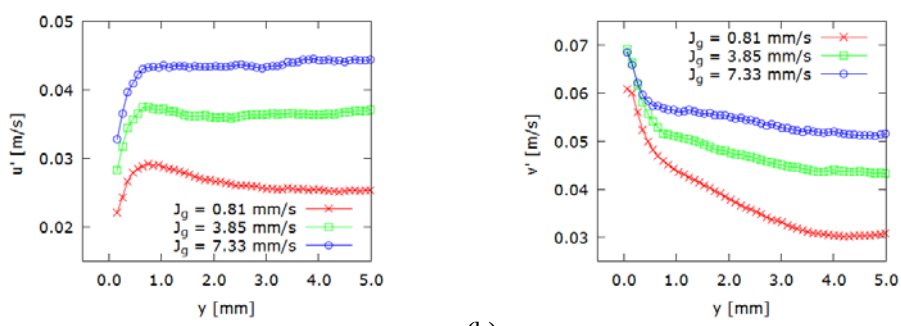

(a) (b)

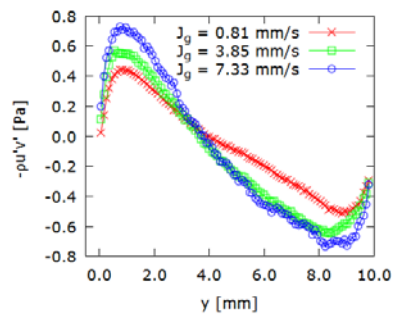

(c)

Figure 9 Liquid flow statistics for different superficial velocities (a) RMS of the axial component of the velocity, (b) RMS of the normal component of the velocity, (c) Reynolds stresses.

Shadowgraphy Results.

Although we require to restrict the measurements only to the bubbly flow regime, multiple gas velocities were implemented. Figure 4 shows examples of the different gas velocities explored. It is important to mention that multiple tests were implemented so as to have an idea of the maximum void fraction that can allow accurate visualization measurements. Visualization techniques are limitted only to low void fractions.

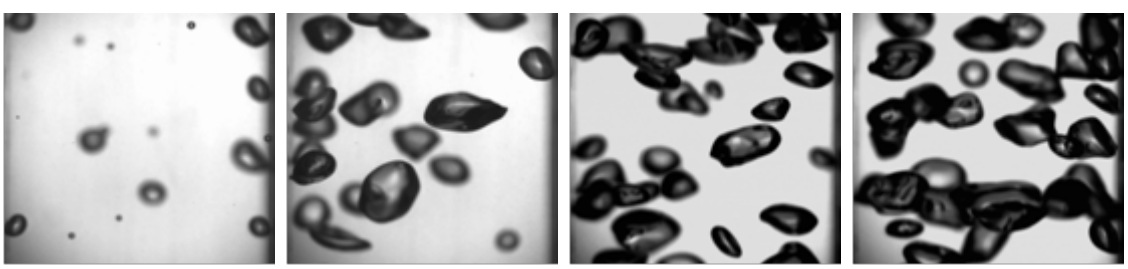

J_g=0.82 mm/s J_g=5.5 mm/s J_g=9.17 mm/s J_g=16.5 mm/s

Figure 10 Examples of Shadowgraphy results from multiple gas velocities.

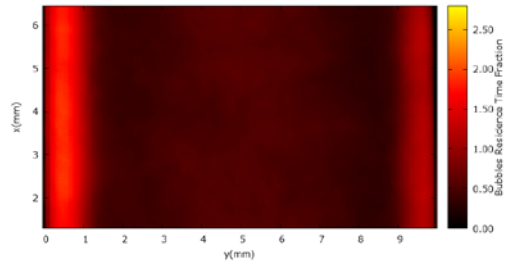

(a) J_g=0.82 mm/s

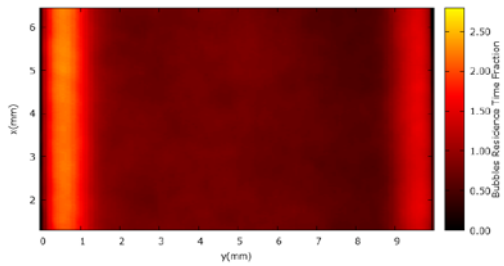

(b) J_g=5.5 mm/s

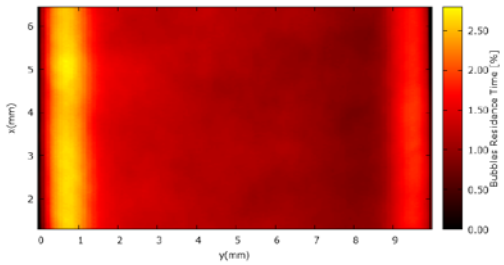

(c) J_g=5.5 mm/s

Figure 11 Residence void fraction measurements from shadowgraphy experimental data for different gas superficial velocities

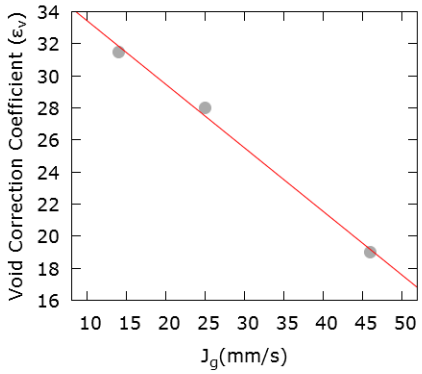

Figure 12 Optical probe void fraction correction factor for visualization measurements

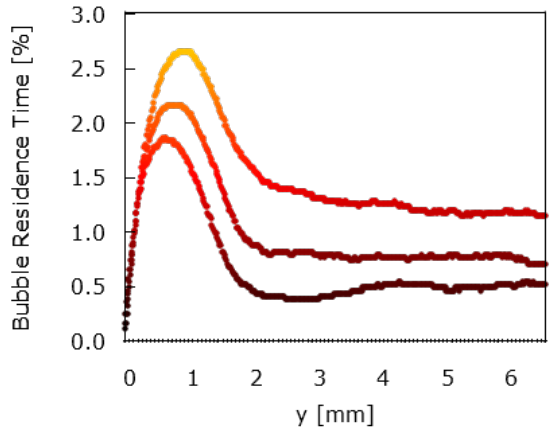

Figure 13 Void fraction profiles estimated from the void residence time fields.

4. CONCLUSIONS

In this work is presented the feasible implementation of whole-field visualization techniques such as Particle Tracking Velocimetry and High speed Shadowgraphy to study isothermal turbulent bubbly flow through a vertical square channel. From the PTV perspective several findings/recommendations are highlighted: For typical bubbly flow experiments, the use of a continuous timing mode has to be used with caution. In two-phase flow conditions, the diluted phase statistics may be hindered due to the lack of independent sampling. The straddling timing mode showed to be superior because it provided higher quality flow statistics. The straddling timing allowed more independent samples to be used on the estimation of the time average quantities. It was also found that large uncertainties on the PTV measurements were induced by the induced reflections of the bubbles, therefore it is recommended to perform simultaneous PTV/Shadowgraphy experiments. The shadowgraphy experiments will dictate the bubbles domain, from which spurious velocity vectors can be removed to reduce this uncertainties. The experimental methodology developed in this work, provided whole-field velocity fields of the two phases, and bubbles dynamics quantification in a simultaneous manner with acceptable accuracy and repeatability. The data gathered using this methodology can be used as an experimental benchmark for validation of CFD codes and for the improvement and development of models and correlations for a better description of two-phase flows.

5. REFERENCES

Colebrook, C.F., 1939. Turbulent Flow in Pipes, with particular reference to the Transition Region between the Smooth and Rough Pipe Laws. *Journal of the ICE*, 11(4), pp.133–156.

Dominguez-Ontiveros, E.E. et al., 2006. Development of a wall shear stress integral measurement and analysis system for two-phase flow boundary layers. *Review of scientific instruments*, 77(10), p.105103.

Durst, F. et al., 1996. Wall shear stress determination from near-wall mean velocity data in turbulent pipe and channel flows. *Experiments in Fluids*, 20(6), pp.417–428.

Estrada-Perez, C. & Hassan, Y., 2010. PTV experiments of subcooled boiling flow through a vertical rectangular channel. *International Journal of Multiphase Flow*, 36(9), pp.691–706.

Gabillet, C., Colin, C. & Fabre, J., 2002. Experimental study of bubble injection in a turbulent boundary layer. *International journal of multiphase flow*, 28(4), pp.553–578.

Hasan, A., Roy, R.P. & Kalra, S.P., 1992. Velocity and temperature fields in turbulent liquid flow through a vertical concentric annular channel. *Int. J. Heat Mass Transfer*, 35(6), pp.1455–1467.

Koncar, B. & Krepper, E., 2008. CFD simulation of convective flow boiling of refrigerant in a vertical annulus. *Nuclear engineering and design*, 238(3), pp.693–706.

Koncar, B. & Tiselj, I., 2010. Influence of near-wall modelling on boiling flow simulation. *Nuclear Engineering and Design*, 240(2), pp.275–283.

Lee, T.H., Park, G.C. & Lee, D.J., 2002. Local flow characteristics of subcooled boiling flow of water in a vertical concentric annulus. *Int. J. Heat Mass Transfer*, 28(8), pp.1351–1368.

Marie, J., Moursali, E. & Tran-Cong, S., 1997a. Similarity law and turbulence intensity profiles in a bubbly boundary layer at low void fractions. *International journal of multiphase flow*, 23(2), pp.227–247.

Marie, J., Moursali, E. & Tran-Cong, S., 1997b. Similarity law and turbulence intensity profiles in a bubbly boundary layer at low void fractions. *International journal of multiphase flow*, 23(2), pp.227–247.

Mikielewicz, D., 2003. Hydrodynamics and heat transfer in bubbly flow in the turbulent boundary layer. *International journal of heat and mass transfer*, 46(2), pp.207–220.

Ramstorfer, F., Steiner, H. & Brenn, G., 2008. Modeling of the microconvective contribution to wall heat transfer in subcooled boiling flow. *Int. J. Heat Mass Transfer*, 51, pp.4069–4082.

Ramstorfer, G. F. Steiner H. Brenn, 2007. Effect of the vapor phase on the near-wall velocity field in subcooled boiling flow. In *Proccedings of the 6th International Conference on Multiphase Flow*.

Roy, R.P. et al., 2002. Turbulent subcooled boiling flow experiments and simulations. *J. Heat Transfer*, 124, p.73.

Roy, R.P., Hasan, A. & Kalra, S.P., 1993. Temperature and velocity fields in turbulent liquid flow adjacent to a bubbly boiling layer. *Int. J. Multiphase Flow*, 19(5), pp.765–795.

Troshko, A. & Hassan, Y., 2001a. A two-equation turbulence model of turbulent bubbly flows. *International Journal of Multiphase Flow*, 27(11), pp.1965–2000.

Troshko, A. & Hassan, Y., 2001b. Law of the wall for two-phase turbulent boundary layers. *International journal of heat and mass transfer*, 44(4), pp.871–875.

Yeoh, G.H. et al., 2002. Prediction and measurement of local two-phase flow parameters in a boiling flow channel. *Num. Heat Transfer, Part A*, 42(1), pp.173–192.